NEOPLASIA
www.neoplasia.com

Volume 17 Number 12 December 2015 pp. 862–870 862

In Vivo Autofluorescence Imaging of Tumor Heterogeneity in Response to Treatment

Amy T. Shah*, Kirsten E. Diggins†, Alex J. Walsh*, Jonathan M. Irish†,‡ and Melissa C. Skala*,†

*Department of Biomedical Engineering, Vanderbilt University, Station B, Box 1631, Nashville, TN, 37235, USA; †Department of Cancer Biology, Vanderbilt University, Nashville, TN 37232, USA; ‡Department of Pathology, Microbiology, and Immunology, Vanderbilt University Medical Center, Nashville, TN 37232, USA

Abstract

Subpopulations of cells that escape anti-cancer treatment can cause relapse in cancer patients. Therefore, measurements of cellular-level tumor heterogeneity could enable improved anti-cancer treatment regimens. Cancer exhibits altered cellular metabolism, which affects the autofluorescence of metabolic cofactors NAD(P)H and FAD. The optical redox ratio (fluorescence intensity of NAD(P)H divided by FAD) reflects global cellular metabolism. The fluorescence lifetime (amount of time a fluorophore is in the excited state) is sensitive to microenvironment, particularly protein-binding. High-resolution imaging of the optical redox ratio and fluorescence lifetimes of NAD(P)H and FAD (optical metabolic imaging) enables single-cell analyses. In this study, mice with FaDu tumors were treated with the antibody therapy cetuximab or the chemotherapy cisplatin and imaged *in vivo* two days after treatment. Results indicate that fluorescence lifetimes of NAD(P)H and FAD are sensitive to early response (two days post-treatment, $P < .05$), compared with decreases in tumor size (nine days post-treatment, $P < .05$). Frequency histogram analysis of individual optical metabolic imaging parameters identifies subpopulations of cells, and a new heterogeneity index enables quantitative comparisons of cellular heterogeneity across treatment groups for individual variables. Additionally, a dimensionality reduction technique (viSNE) enables holistic visualization of multivariate optical measures of cellular heterogeneity. These analyses indicate increased heterogeneity in the cetuximab and cisplatin treatment groups compared with the control group. Overall, the combination of optical metabolic imaging and cellular-level analyses provide novel, quantitative insights into tumor heterogeneity.

Neoplasia (2015) 17, 862–870

Introduction

Cancer treatments often include chemotherapy, targeted therapy, and/or radiation therapy. Most cancer patients respond to treatment initially, exhibiting decreased tumor size, and later relapse, exhibiting increased tumor size. Chemotherapy and targeted treatments can eliminate the majority of cells in a tumor while subpopulations of cells can escape treatment [1,2]. These subpopulations of cells may be responsible for innate or acquired resistance, which can enable treatment failure, disease progression, and diminished patient outcomes.

Standard chemotherapies and radiation treatments are administered based on average response rates for a particular type and stage of cancer. Current methods for determining targeted treatment strategies rely on identifying the dominant subpopulation of cells, usually based on surface marker expression, and administering drugs that inhibit the overexpressed targets to decrease proliferation or increase death of the cells expressing those targets [3]. Resistant subpopulations existing within a tumor could escape the treatment, allowing relapse after therapy. Therefore, tumor heterogeneity poses a difficult challenge for optimizing treatment outcomes in cancer patients.

Address all correspondence to: Melissa C. Skala, PhD, Assistant Professor, Department of Biomedical Engineering, Vanderbilt University, Station B, Box 351631, Nashville, TN 37235.
E-mail: m.skala@vanderbilt.edu
Received 24 August 2015; Revised 11 November 2015; Accepted 16 November 2015

1476-5586
http://dx.doi.org/10.1016/j.neo.2015.11.006

Tumor heterogeneity can be characterized as genetic, phenotypic, or functional [4,5]. Genetic measures focus on analysis of genes known to promote tumor progression. Phenotypic characterization is usually established from histology to visualize cell morphology and from immunohistochemistry to measure expression of cell surface receptors, growth factors, and hormone receptors. However, these measures may not directly relate to cellular function [4]. Whereas genetic and phenotypic biomarkers provide static measurements, functional measures characterize dynamic tumor behavior or response to stimuli and therefore may be more attractive. Functional measures include cellular metabolism, oxygen consumption, and blood perfusion. In particular, cellular metabolism, which is altered in cancer [6], has been shown to be a good indicator of drug response and therefore may be a promising marker for tumor heterogeneity [7].

Numerous metabolic pathways involve the autofluorescent co-enzymes NAD(P)H (an electron donor) and FAD (an electron acceptor). The optical redox ratio is defined as the fluorescence intensity of NAD(P)H divided by that of FAD, and is an established method for monitoring relative amounts of electron donor and acceptor in a cell [8–10]. As a complementary measure, the fluorescence lifetime reports the amount of time a fluorophore is in the excited state before relaxing to the ground the state. Fluorescence lifetime is sensitive to conformational changes in enzyme structure that are caused by the microenvironment, particularly protein-binding [11]. The fluorescence lifetime of NAD(P)H has two distinct components, due to vastly different lifetimes when NAD(P)H is in the free and protein-bound states [12]. Similarly, FAD has two lifetimes due to its free and protein-bound states [13]. The short lifetimes of NAD(P)H (free state) and FAD (protein-bound state) are due to quenching by the adenine moiety of the molecule [11]. The redox ratio and fluorescence lifetime provide independent measurements of cellular metabolism [10], and can be performed using two-photon fluorescence microscopy, which enables cellular-level imaging and deeper penetration in tissue than single-photon (e.g. confocal) microscopy [14]. This approach exploits the endogenous contrast of NAD(P)H and FAD autofluorescence to acquire quantitative measurements of cellular metabolism that can be used to characterize cellular heterogeneity.

There are few analysis approaches that are appropriate for quantifying cellular heterogeneity. The Shannon diversity index is a metric used in ecology literature that incorporates the number and relative proportions of species in a community [15], and it has also been applied to tumor heterogeneity [16–18]. However, the degree of separation between subpopulations is also an important consideration in tumor heterogeneity [19], which is not incorporated into the Shannon diversity index. A metric incorporating the number of cellular subpopulations, relative contributions of each subpopulation, and relative differences in subpopulations to quantify tumor heterogeneity could provide insight into optimal treatment strategies for cancer patients. This type of metric could be applied to each optical metabolic imaging parameter, including the redox ratio and fluorescence lifetime components of NAD(P)H and FAD.

Since optical metabolic imaging acquires multi-dimensional data sets of parameters, which can be difficult to interpret holistically, dimensionality reduction techniques can be applied as a complementary method to facilitate interpretation of these types of data sets. Traditional methods apply a linear transformation of the data, like principal component analysis [20]. However, an alternative method that preserves nonlinear relationships at a single-cell level may be advantageous, like the viSNE technique [21]. viSNE is a dimensionality reduction tool that uses t-distributed stochastic neighbor embedding (t-SNE) to plot high-dimensional single-cell data on a two-dimensional axis for visualization of cellular heterogeneity, and is well-suited for single-cell data acquired in optical metabolic imaging. viSNE is also attractive for identifying cell sub-populations because it preserves the relative distances between cells that are present in multi-dimensional space when projecting them into two-dimensional space, thereby maintaining relationships between individual cells in the reduced data set and identifying relationships that would not be apparent by manual analysis alone.

This study quantifies the optical redox ratio and fluorescence lifetimes of NAD(P)H and FAD in a xenograft model of head and neck cancer two days after treatment with the antibody therapy cetuximab or the chemotherapy cisplatin. Additionally, these *in vivo* high-resolution images enabled analysis of cellular metabolic heterogeneity in response to treatment at an early time point using endogenous contrast. An index to quantify heterogeneity was developed, validated on samples containing cultures of one cell line or co-cultures containing two cell lines, and applied *in vivo* to each individual optical metabolic imaging variable. Additionally, a dimensionality reduction technique (viSNE) was applied to enable holistic visualization of heterogeneity across all optical metabolic imaging variables combined. Immunohistochemistry stains for cell proliferation and cell death validated treatment efficacy, and tumor growth curves measured gold standard treatment response. Results indicate that *in vivo* optical metabolic imaging, combined with a quantitative metric of heterogeneity or a dimensionality reduction visualization of heterogeneity, has potential to resolve treatment-induced cellular-level heterogeneities in tumors. Ultimately, characterization of cellular heterogeneity could enable optimized treatment regimens and improved patient outcomes.

Materials and Methods

In Vivo Imaging and Tumor Growth Curves

FaDu cells were grown in DMEM media supplemented with 10% fetal bovine serum (FBS) and 0.4 μg/mL hydrocortisone. Approximately 10^7 FaDu cells were injected into the flanks of 7 week old male nude mice and tumors were grown to approximately 100 mm^3. Mice in treated groups received treatment of cetuximab (33 mg/kg) [22,23] or cisplatin (6 mg/kg) [24] via intraperitoneal injection. To measure tumor growth curves, mice were treated three times a week for two weeks (6 tumors per group). Tumor sizes were measured daily and calculated by $(l*w^2)/2$, where l represents the tumor length in mm and w represents the tumor width in mm. Tumor sizes were normalized to the size on day 1. On day 13, tumors were excised and fixed for immunohistochemistry, and mice were euthanized. A separate cohort of mice was used for *in vivo* imaging studies, with only one dose per treatment group on day zero (6 tumors for control group, 5 tumors for cetuximab and cisplatin groups). Two days after treatment, each mouse was anesthetized and the skin covering the tumor was removed. A coverslip was placed over the exposed tumor, and the mouse was placed on the microscope to acquire *in vivo* images (3–7 images per tumor).

Imaging Instrumentation

Mice were imaged on a custom-built (Bruker) inverted two-photon fluorescence microscope (Ti-E Nikon) using a 40× oil immersion objective (1.3 NA). A titanium:sapphire laser (Chameleon, Coherent

Inc.) was used for excitation, and a GaAsP photomultiplier tube (H7422P-40, Hamamatsu) was used for fluorescence collection. To measure NAD(P)H autofluorescence, an excitation wavelength of 750 nm and an emission filter of 400 to 480 nm was used. To measure FAD autofluorescence, an excitation wavelength of 890 nm and an emission filter of 500 to 600 nm was used. Time correlated single photon counting electronics (SPC-150, Becker and Hickl) were used to acquire fluorescence lifetime images over 60 seconds, and photon count rates (~ 2 to 3 × 10^5) were monitored during this time to ensure the absence of photobleaching. A pixel dwell time of 4.8 μs was used to acquire 256 × 256 pixel images. First, an NAD(P)H lifetime image was acquired, and then an FAD lifetime image was acquired from the same field of view. Sequential fields of view were separated by at least one field of view. A Fluoresbrite YG microsphere (Polysciences Inc.) was imaged as a daily standard with a fluorescence lifetime of 2.11 ± 0.05 ns (n = 7), consistent with previous studies [25,26]. Instantaneous scattering from second harmonic generation of urea crystals excited at 900 nm was measured to calculate the full width at half maximum of the instrument response function (244 ps).

Image Analysis

Fluorescence lifetime images were analyzed as described previously [27]. Briefly, the fluorescence lifetime decay curves were fit to a two-component exponential function, $F(t) = \alpha_1 e^{-t/\tau 1} + \alpha_2 e^{-t/\tau 2} + c$, where F(t) represents the fluorescence intensity over time, α_1 and α_2 represent the contribution from the short and long lifetime components respectively ($\alpha_1 + \alpha_2 = 1$), and τ_1 and τ_2 represents the fluorescence lifetime of the short and long lifetime components respectively (SPCImage, Becker and Hickl). A two-component fit has been shown to be appropriate for describing freely diffusing versus protein-bound conformations of NAD(P)H and FAD [25]. For NAD(P)H, the short lifetime represents free NAD(P)H, and for FAD the short lifetime represents protein-bound FAD [11]. The weighted mean lifetime, τ_m, was calculated by $\tau_m = \alpha_1\tau_1 + \alpha_2\tau_2$. A fluorescence intensity image was generated by integrating the fluorescence lifetime decay over time for each pixel in the lifetime image. The optical redox ratio was calculated by dividing the NAD(P)H fluorescence intensity by the FAD fluorescence intensity for each pixel to create a redox ratio image for each field of view. NAD(P)H and FAD fluorescence specific to cellular metabolism is localized in the cytoplasm and mitochondria. Therefore, the redox ratio and fluorescence lifetime images were thresholded to remove nuclear fluorescence, and the average redox ratio and fluorescence lifetime decay parameters for each remaining cell cytoplasm was computed. The optical redox ratio and NAD(P)H and FAD fluorescence lifetime images were quantified for each cytoplasm in each cell using a customized CellProfiler routine as described previously [28].

Heterogeneity Index and Validation

For subpopulation analysis, frequency histograms were plotted for the optical redox ratio, NAD(P)H τ_m, and FAD τ_m, as described and validated in [29]. The histograms were fit to one-, two-, or three-component Gaussian curves, and the lowest Akaike Information Criterion indicated optimal fitting [8]. Each Gaussian curve represents a subpopulation of cells, and the sum of the Gaussian curves was plotted for visualization. To quantify heterogeneity, a heterogeneity index was defined as $H = -\sum d_i p_i \ln p_i$, where i represents each subpopulation, d represents the distance between the median of the subpopulation and the median of all data within a group, and p represents the proportion of the subpopulation. Validation of the heterogeneity index was performed on co-cultures of MDA-MB-231 and SKBr3 breast cancer cell lines plated at ratios of 0:100, 50:50, and 100:0.

viSNE

The viSNE dimensionality reduction tool was used to visualize cellular heterogeneity by incorporating all seven optical metabolic imaging parameters: the optical redox ratio, NAD(P)H α_1, NAD(P)H τ_1, NAD(P)H τ_2, FAD α_2, FAD τ_1, and FAD τ_2. The data from each parameter was transformed to a common scale of 0 to 100%, where 100% represented the highest value for that parameter across all treatment groups. Data were analyzed in Cytobank (www.cytobank.org) to create a viSNE map [21,30,31]. viSNE performs t-distributed stochastic neighbor embedding (t-SNE) to minimize the differences between high-dimensional space and low-dimensional space, and produces a two-dimensional plot in arbitrary units. Briefly, a pairwise distance matrix is calculated in high dimensional space, which is transformed to a similarity matrix using a varying Gaussian kernel. The points are randomly mapped in low-dimensional space and iteratively rearranged to minimize the divergence between high-dimensional and low-dimensional similarity matrices.

Statistical Analyses

Bar graphs are shown as mean ± standard error. Kruskal-Wallis and two-way rank sum tests determined statistical significance with an α of 0.05.

Results

Tumor growth curves measure tumor size changes in FaDu xenografts after treatment (Figure 1*A*). Compared with control, cetuximab and cisplatin treatments cause tumor size decreases starting six and nine days, respectively after treatment onset ($P < .05$). Immunohistochemistry was performed on excised tumor tissue at the end of the study to quantify markers of treatment efficacy (Figure 1). Ki-67 staining shows decreased proliferation with each treatment group ($P < .05$; Figure 1*B*). Cleaved caspase 3 shows increased cell death with cisplatin treatment ($P < .05$; Figure 1*C*). These gold standard measurements verify drug efficacy in the xenografts.

Representative *in vivo* images demonstrate cellular-level resolution of NAD(P)H and FAD autofluorescence imaging and enables visualization of qualitative differences in the optical metabolic imaging parameters two days after treatment (Figure 2). Images were quantified to calculate the average optical redox ratio, NAD(P)H fluorescence lifetime, and FAD fluorescence lifetime per-cell (Figure 3). The redox ratio shows no change with cetuximab treatment and decreases with cisplatin treatment ($P < .05$). The NAD(P)H fluorescence lifetime decreases with cetuximab and cisplatin treatments ($P < .05$). The FAD fluorescence lifetime decreases with cetuximab and cisplatin treatments ($P < .05$). The shifts in fluorescence lifetime reflect shifts in microenvironment, particularly NAD(P)H and FAD protein-binding. NAD(P)H τ_1, NAD(P)H τ_2, FAD τ_1, and FAD τ_2 decrease with cetuximab and cisplatin treatments (Supplementary Figure 1, $P < .05$). The relative amounts of free NAD(P)H and FAD increase and decrease, respectively, with cetuximab and cisplatin treatments (Supplementary Figure 1, $P < .05$).

Single-cell images were represented as histograms of number of cells versus optical metabolic imaging parameters, and Gaussian fits were used to identify distinct cell sub-populations for each treatment group. Histograms plotting the sum of Gaussian fits for the redox

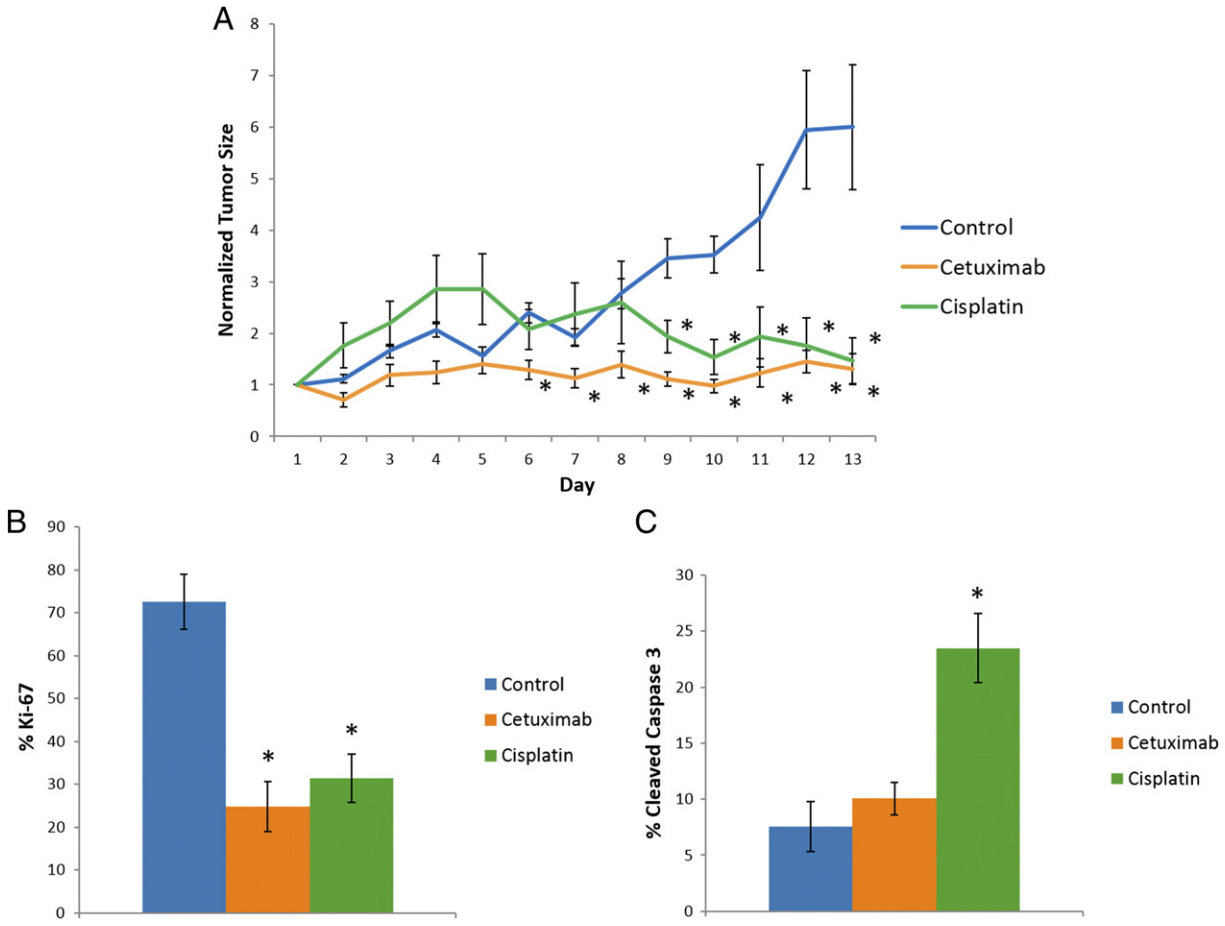

Figure 1. (A) Tumor growth curves show a decrease (*$P < .05$, compared with control) in tumor size in cetuximab treated xenografts after 6 days of treatment and in cisplatin treated xenografts after 9 days of treatment. Xenografts were excised and stained for ki-67 (proliferation) and cleaved caspase 3 (cell death) on day 13. (B) Xenografts from cetuximab and cisplatin treated mice exhibited decreased proliferation. (C) Xenografts from cisplatin treated mice exhibited increased cell death. *$P < .05$ compared with control, rank sum test.

ratio, NAD(P)H fluorescence lifetime, and FAD fluorescence lifetime highlight cellular heterogeneity across treatment groups for each optical parameter (Figure 4, *A–C* and Supplementary Figure 2). For the redox ratio, histograms of the treatment groups have some overlap with control. This trend is consistent with the NAD(P)H and FAD fluorescence lifetimes. The degree of overlap for the subpopulations of cells from each treatment group compared with control could reflect the degree of resistant cells compared with responsive cells.

In order to compare cellular-level heterogeneity across treatment groups, a quantitative metric called the "heterogeneity index" was developed, validated *in vitro*, and then applied to *in vivo* histograms. The heterogeneity index is the Shannon diversity index weighted by a distance factor, where a larger value indicates more subpopulations, similar numbers of cells within each subpopulation, and/or more distance between subpopulations. The heterogeneity index was validated on co-cultures of MDA-MB-231 and SKBr3 breast cancer cell lines because they exhibit distinct optical redox ratios [10]. The heterogeneity index was calculated for the optical redox ratio of dishes including 100% MDA-MB-231 cells, 100% SKBr3 cells, and 50% MDA-MB-231 + 50% SKBr3 cells. The condition with two cell lines causes an increased heterogeneity index (0.285) compared with the MDA-MB-231 cell line (0.006) or the SKBr3 cell line (0.152) cultured alone (Table 1), indicating that the heterogeneity index behaves as expected. SKBr3 cells have been shown to exhibit intrinsic heterogeneity within the cell line based on HER2 expression, which could account for the relatively high heterogeneity index within that cell line [32]. For the *in vivo* studies, the heterogeneity index is increased for the treated groups compared with the control for the redox ratio (Figure 4*A*), NAD(P)H fluorescence lifetime (Figure 4*B*), and FAD fluorescence lifetime (Figure 4*C*). This trend in heterogeneity index is consistent for the redox ratio of FaDu cell monolayers treated with cetuximab and cisplatin *in vitro* (Supplementary Figure 4). Note that the heterogeneity index is not normalized, and therefore not comparable between variables.

The heterogeneity index is helpful to analyze individual variables, but a dimensionality reduction technique is necessary to visualize tumor heterogeneity with respect to all optical variables combined. viSNE reduces seven optical metabolic imaging parameters by preserving the similarities across cells and projecting these onto a two-dimensional axis (Figure 5). viSNE analysis shows a distinct population of the control group, while the cetuximab and cisplatin treatment groups overlap with control and also exhibit a separate subpopulation of cells (Figure 5*A*). This trend is consistent in FaDu cell monolayers *in vitro* (Supplementary Figure 4). viSNE preserves similarities across cells in a nonlinear way by producing a visual two-dimensional scatter plot, but does not provide a quantitative relationship between the input parameters and the

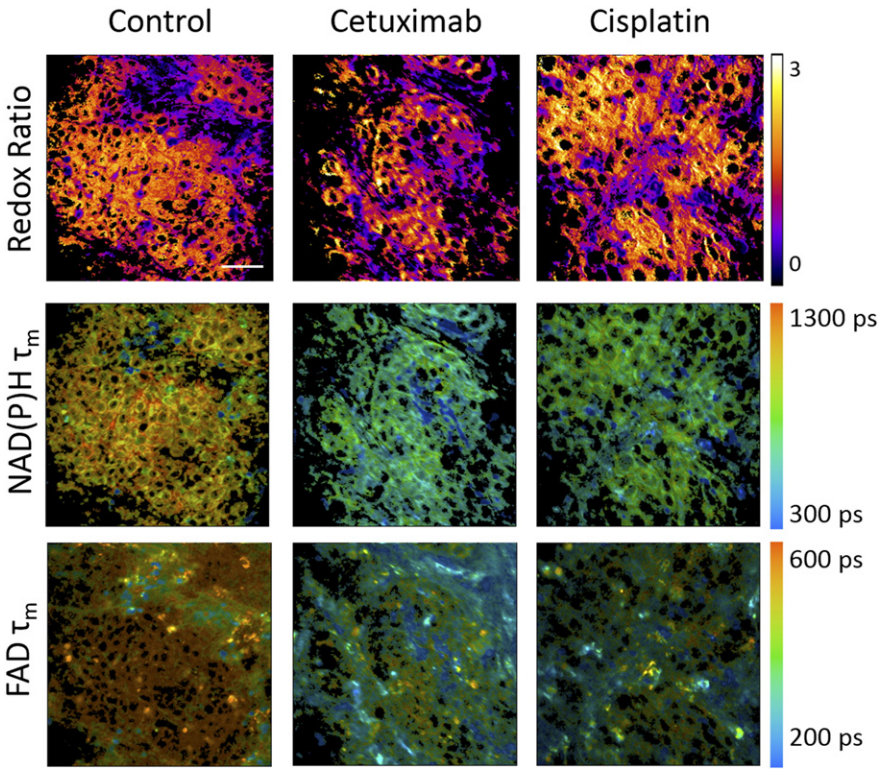

Figure 2. *In vivo* images of FaDu xenografts 2 days after treatment with cetuximab or cisplatin. NAD(P)H and FAD autofluorescence images were acquired from the same fields of view, and the redox ratio (top row), NAD(P)H fluorescence lifetime (middle row), and FAD fluorescence lifetime (bottom row) were calculated. Scale bar = 50 μm.

viSNE plot. Therefore, heat maps plotting the values for individual parameters over the two-dimensional viSNE axes can be helpful for understanding the contribution of each parameter to the viSNE plot (Figure 5, *B* and *C* and Supplementary Figure 3). Gradients within a parameter that correspond with the grouping in the viSNE plot indicate that these parameters contribute significantly to the viSNE plot. In particular, gradients in NAD(P)H τ_1 and FAD τ_1 agree with grouping in the viSNE plot because points in the top group of the viSNE plot exhibit low values compared with points in the bottom group (Figure 5, *B* and *C*).

Discussion

Tumor heterogeneity poses a difficult challenge for improving treatment outcomes in cancer patients. The goal of this study is to apply autofluorescence imaging of the metabolic cofactors NAD(P)H and FAD to resolve anti-cancer treatment response on a cellular level, and characterize cellular heterogeneity. Mice with FaDu xenografts were treated with cetuximab or cisplatin, and 48 hours later the xenografts were imaged *in vivo* using two-photon microscopy and fluorescence lifetime imaging. Cellular-level imaging enabled per-cell analysis of the optical redox ratio and fluorescence lifetimes of NAD(P)H and FAD in response to treatment, and a heterogeneity index was devised to quantify cellular heterogeneity for each optical metabolic imaging variable. Furthermore, a dimensionality reduction technique was applied on a per-cell level to visualize heterogeneity on a two-dimensional axis based on combined information from all optical variables. Overall, the degree of heterogeneity is increased for the xenografts of mice treated with cetuximab or cisplatin compared with control. These nondestructive, quantitative methods to measure *in vivo* cellular heterogeneity could be used to develop improved treatments that account for tumor heterogeneity and target all tumor cell sub-populations for improved efficacy in cancer patients.

Tumor growth curves show that over two weeks of treatment the administration of cetuximab or cisplatin causes stable disease, exhibiting decreased tumor size compared with control tumors that exhibit continued increase in tumor size (Figure 1*A*). These results agree with clinical studies of patients administered cetuximab or cisplatin [33,34]. Additionally, cetuximab and cisplatin treatment cause decreased cell proliferation (Figure 1*B*), which agrees with previous *in vitro* studies [35,36]. Cisplatin treatment causes increased cell death (Figure 1*C*). Cisplatin has been shown to cause apoptosis [37], and cetuximab sensitizes cells to chemotherapy by inhibiting DNA repair mechanisms [38]. Cetuximab has been shown to cause autophagy instead of apoptosis [35]. These immunohistochemistry measures verify *in vivo* drug efficacy.

The redox ratio of FaDu xenografts measured *in vivo* decreases 48 hours after cisplatin treatment, whereas cetuximab treatment causes no change in the redox ratio (Figure 3*A*). These results agree with *in vitro* optical redox ratio measurements in SCC25 and SCC61 head and neck cancer cell lines treated with cetuximab or cisplatin [27]. The lack of effect from cetuximab treatment could reflect its administration as a single agent, since cetuximab is maximally effective in combination with chemotherapy and radiation therapy. Additionally, cetuximab initiates antibody-dependent cell cytotoxicity (ADCC), but this process might be altered in the immunocompromised nude mice used in this study [39]. The NAD(P)H and FAD mean lifetimes decrease with cetuximab and cisplatin treatment (Figure 3, *B* and *C*), which could reflect treatment-induced changes

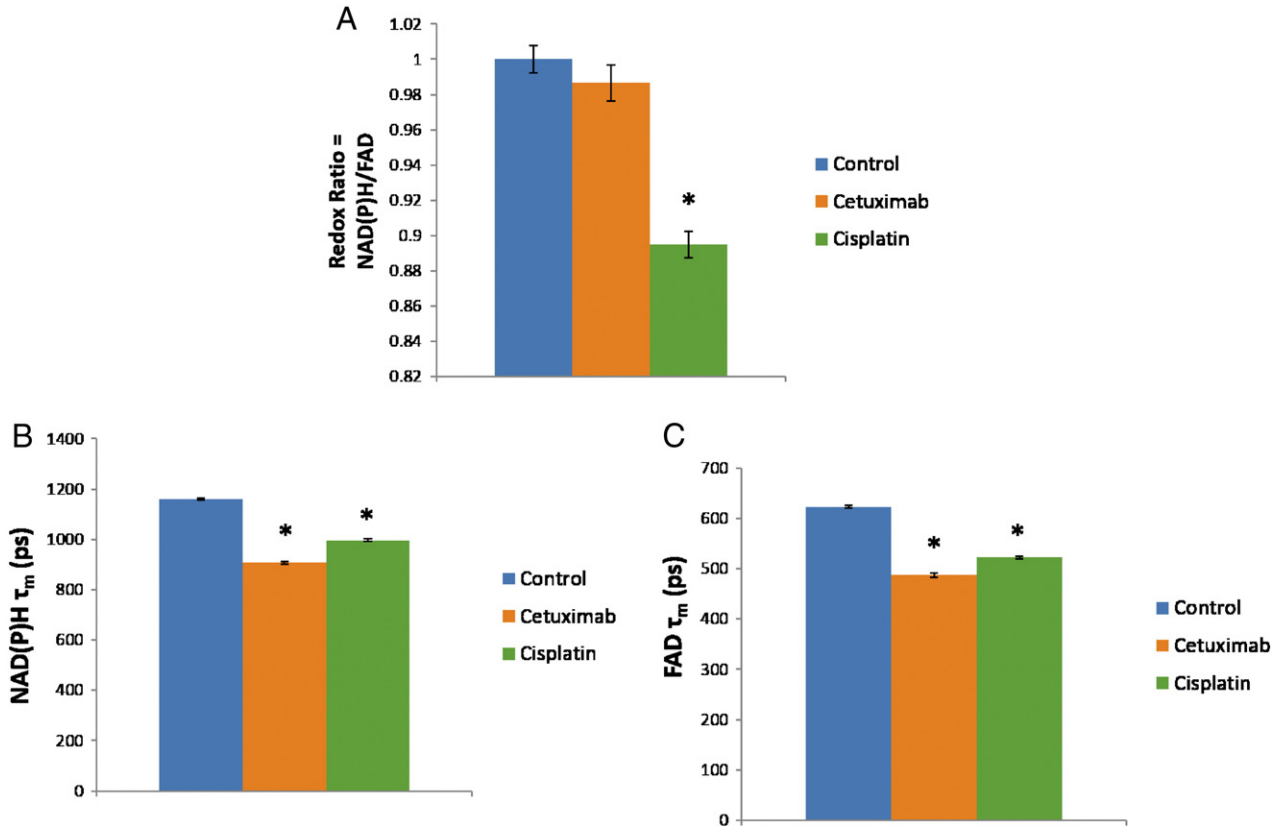

Figure 3. The optical redox ratio, NAD(P)H fluorescence lifetime, and FAD fluorescence lifetime were quantified on a per-cell level from *in vivo* NAD(P)H and FAD autofluorescence images 2 days after treatment. (A) The redox ratio decreases with cisplatin treatment. (B, C) The NAD(P)H and FAD fluorescence lifetimes decrease after cetuximab and cisplatin treatment. The shifts in NAD(P)H and FAD fluorescence lifetime measured 2 days after treatment are consistent with response measure by tumor growth curves and immunohistochemistry after 13 days of treatment. *$P < .05$, compared with control.

in preferred metabolic pathways involving NAD(P)H and FAD. These results also highlight the fact that the redox ratio and fluorescence lifetimes of NAD(P)H and FAD probe different features of cellular metabolism [10]. The redox ratio reflects relative amounts of electron donor (NAD(P)H) and acceptor (FAD), whereas the fluorescence lifetimes of NAD(P)H and FAD reflect enzyme activity, preferred protein-binding, and other microenvironmental factors (e.g. pH) of these co-factors [11]. Decreased NAD(P)H and FAD mean fluorescence lifetimes have also been measured in BT474 breast cancer xenografts treated with antibody therapy trastuzumab two days after treatment [10]. No previous literature has reported the effects of chemotherapy *in vivo* on the optical redox ratio and fluorescence lifetimes of NAD(P)H and FAD. These fluorescence lifetime changes two days after treatment agree with tumor size decreases in treated mice nine days after treatment onset, indicating that NAD(P)H and FAD fluorescence lifetime measurements could reflect early treatment-induced metabolic effects.

To visualize treatment-induced shifts in cellular heterogeneity, frequency histograms were plotted for the optical redox ratio and mean fluorescence lifetimes of NAD(P)H and FAD. Shifts in the histograms can be qualitatively visualized across control and treatment groups (Figure 4), and a metric to describe cellular heterogeneity is necessary for quantitative comparisons. However, there is no standard metric for quantifying tumor heterogeneity. We have modified the Shannon diversity index to incorporate the relative separation between subpopulations by including a coefficient of the distance between the median of each subpopulation to the median of the group. Since the scale and range of this coefficient depends on the parameter, the heterogeneity index is a relative value for each parameter. A heterogeneity index of 0 indicates one population of cells, and the index increases with increased number of subpopulations, evenness between subpopulations, and distance between subpopulations. The heterogeneity index increases for co-cultures of SKBr3 and MDA-MB-231 cells compared with either cell line alone (Table 1), indicating that an increased heterogeneity index reflects increased sample heterogeneity. The heterogeneity index was calculated for the redox ratio, NAD(P)H fluorescence lifetime, and FAD fluorescence lifetime (Figure 4), and is consistently lower for the control group compared with the cetuximab or cisplatin treatments. The higher heterogeneity index for the treatments indicates increased variability in cellular response to each treatment, and could indicate a balance between cellular response and resistance that leads to stable disease as seen in tumor growth curves (Figure 1*A*). Additionally, *in vitro* heterogeneity analysis of FaDu cell monolayers show similar response as *in vivo* results, indicating intrinsic heterogeneity in the FaDu cell response to cetuximab and cisplatin (Supplementary Figure 4). Other factors could also contribute to *in vivo* drug response, including hypoxia, drug delivery, and glucose gradients. These factors could induce greater heterogeneity in the *in vivo* optical metabolic imaging measurements compared to *in vitro* measurements.

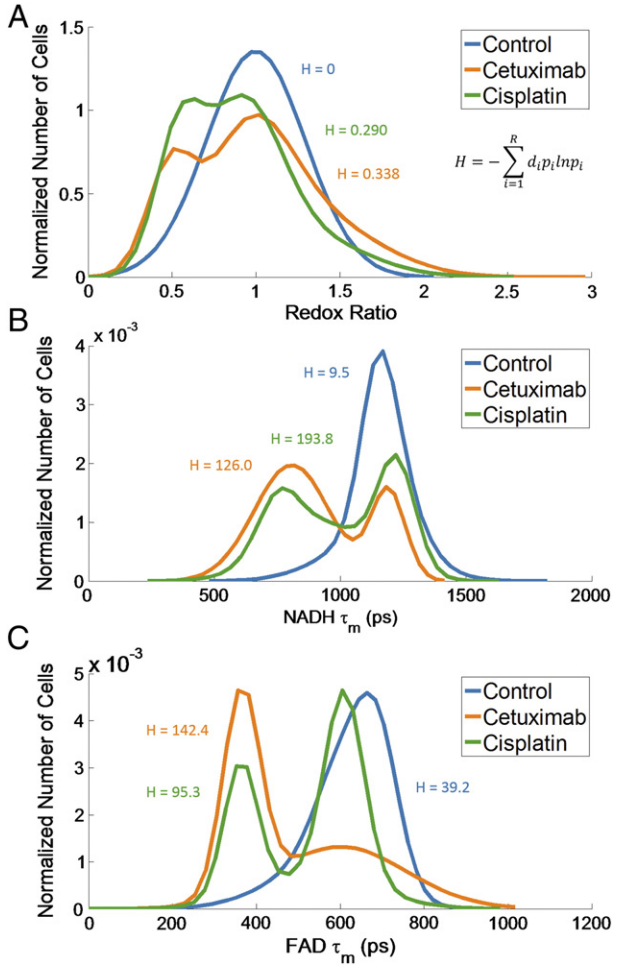

Figure 4. To quantify the level of cellular metabolic heterogeneity within a treatment group, each group is fit to one, two, or three Gaussian curves based on the Akaike Information Criterion. Each Gaussian curve represents one subpopulation, and the sum of the Gaussian curves is plotted for visualization. The heterogeneity index, *H*, is a weighted sum over each subpopulation within a treatment group that incorporates *d*, the distance between the median of the subpopulation and the median of all data in the treatment group, and *p*, the weight of the subpopulation. This parameter is the Shannon diversity index modified to incorporate the relative location of each subpopulation. Increased heterogeneity index indicates increased number of subpopulations, increased equality in the weights of each subpopulation within a treatment group, and increased separation in the locations of the subpopulations. (A) The heterogeneity index for the redox ratio is lowest for the control group followed by the cisplatin and cetuximab treatment groups. (B) The heterogeneity index for the NAD(P)H fluorescence lifetime is lowest for the control group followed by the cetuximab and cisplatin treatment groups. (C) The heterogeneity index for the FAD fluorescence lifetime is lowest for the control group followed by the cisplatin and cetuximab treatment groups.

The heterogeneity index can be applied to individual optical metabolic imaging parameters. However, since the seven optical metabolic imaging parameters are complementary measures [10], incorporating all parameters into one heterogeneity analysis could provide additional insight for characterizing tumor heterogeneity. Dimensionality reduction techniques can preserve the similarity between cells across multiple variables, and project relative distances between cells onto a two-dimensional scatter plot. Common dimensionality reduction techniques include principal component analysis, but this method requires a linear transformation of the data [40]. The viSNE technique optimizes the separation between cells based on high-dimensional data sets without relying on a linear transformation of the data, so it can preserve non-linear relationships at single-cell resolution, identify rare subpopulations of cells, and provide a two-dimensional plot for visualization of cellular heterogeneity [21]. These advantages make viSNE an attractive tool for the analysis of optical metabolic imaging parameters. viSNE analysis shows a distinct population of cells in the control group. In contrast, the cetuximab and cisplatin treatment groups overlap with control and also display a separate subpopulation of cells (Figure 5). This indicates increased heterogeneity in the treatments compared with the control, which agrees with the analysis of the heterogeneity index applied to individual optical metabolic imaging parameters (redox ratio, NAD(P)H and FAD fluorescence lifetimes). A gradient in the short lifetime components of NAD(P)H and FAD can be seen across the viSNE map (Figure 5, *B* and *C*), which indicates that these optical parameters contribute more variability to the data set. These results indicate that the combination of optical metabolic imaging and single-cell analyses (heterogeneity index, viSNE) are attractive for characterizing tumor heterogeneity.

Table 1. Validation of the Heterogeneity Index

MDA-MB-231: SKBr3 Ratio	0:100	50:50	100:0
Heterogeneity Index	0.152	0.285	0.006

The heterogeneity index is defined as $H = -\sum[d_i p_i \ln(p_i)]$, where i represents each subpopulation, *d* represents the distance between the median of the subpopulation and the median of all data within a group, and p represents the proportion of the subpopulation. The heterogeneity index was validated using redox ratio measurements of MDA-MB-231 and SKBr3 cell monolayer cultures plated at ratios of 0:100, 50:50, and 100:0, and exhibits an increased value for the 50:50 condition.

Tumor heterogeneity poses a challenge for optimizing anti-cancer treatment strategies in cancer patients, and new tools are necessary to adequately quantify and interpret tumor heterogeneity *in vivo* in animal models at a cellular level. This study shows that optical metabolic imaging can resolve metabolic shifts induced by chemotherapy and targeted therapy *in vivo* at an early time point. Autofluorescence imaging on a cellular level is well-suited for analysis of heterogeneity across single cells. In particular, a heterogeneity index can quantify drug-induced shifts in heterogeneity across treatment groups for individual variables, and dimensionality reduction techniques can be advantageous for holistic interpretation of multivariate measures of cellular heterogeneity. These methods for assessing tumor heterogeneity could enable improved treatment regimens that account for tumor heterogeneity, leading to improved outcomes for cancer patients.

Supplementary data to this article can be found online at http://dx.doi.org/10.1016/j.neo.2015.11.006.

Acknowledgements

The Vanderbilt University Translational Pathology Shared Resource was used for immunohistochemistry staining. Funding sources include the NIH R01 CA185747 (M.C.S.), DoD W81XWH-13-1-0194 (M.C.S.), Mary Kay Foundation 067–14 (M.C.S.), NSF Graduate Research Fellowship DGE-0909667 (A.T.S.), NIH/NCI R25 CA136440-04 (K.E.D.), R00 CA143231-03 (J.M.I.), the Vanderbilt-Ingram Cancer Center (VICC, P30 CA68485), and VICC Ambassadors (J.M.I., M.C.S.).

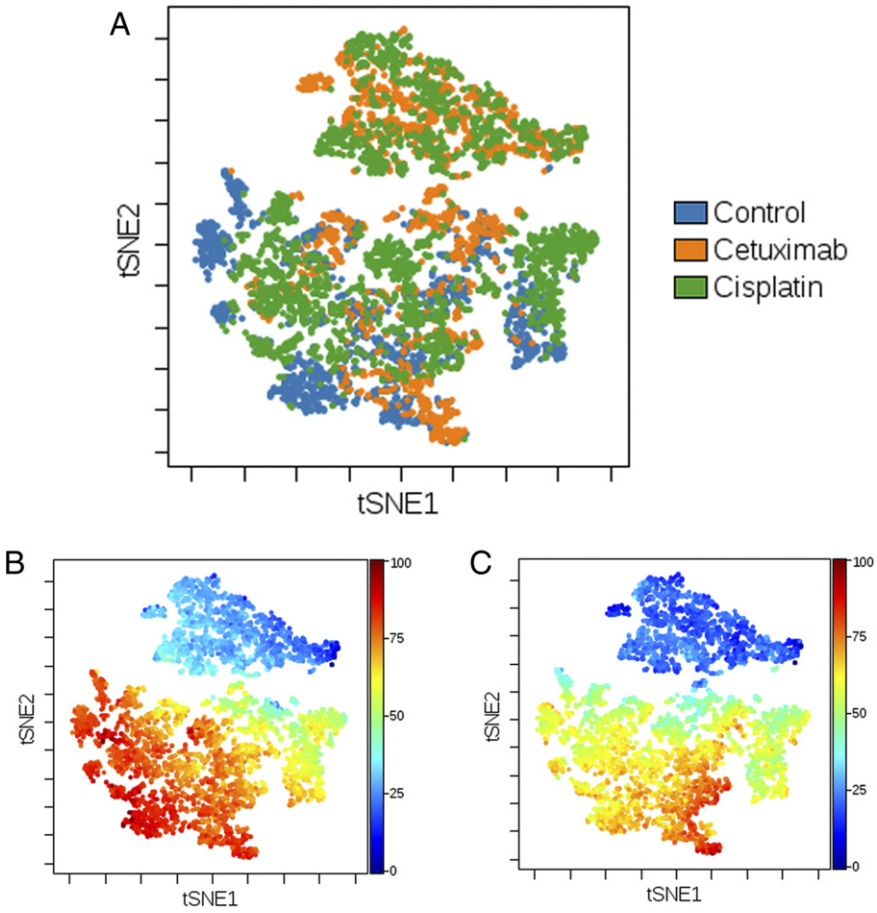

Figure 5. Single-cell analysis using the dimensionality-reduction technique viSNE reduces seven optical metabolic imaging parameters to two dimensions for visualization of heterogeneity across individual cells. To account for different scales between parameters, common linear transformation was applied within each parameter across all treatment groups so the transformed values range from 0 to 100. (A) viSNE analysis shows a distinct population of cells for the control group. The cetuximab and cisplatin treatment groups overlap with the control group and also exhibit a separate subpopulation of cells. (B, C) Heat maps of the short fluorescence lifetime components for (B) NAD(P)H and (C) FAD show gradients over the 2-dimensional viSNE axes.

References

[1] Khong HT and Restifo NP (2002). Natural selection of tumor variants in the generation of 'tumor escape' phenotypes. *Nat Immunol* **3**(11), 999–1005.

[2] Puig P, Guilly M, Bouchot A, Droin N, Cathelin D, Bouyer F, Favier L, Ghiringhelli F, Kroemer G, and Solary E, et al (2008). Tumor cells can escape DNA-damaging cisplatin through DNA endoreduplication and reversible polyploidy. *Cell Biol Int* **32**(9), 1031–1043.

[3] Zhao B, Hemann MT, and Lauffenburger DA (2014). Intratumor heterogeneity alters most effective drugs in designed combinations. *Proc Natl Acad Sci U S A* **111**(29), 10773–10778.

[4] Marusyk A and Polyak K (2010). Tumor heterogeneity: causes and consequences. *Biochim Biophys Acta* **1805**(1), 105–117.

[5] Hanahan D and Weinberg RA (2011). Hallmarks of cancer: the next generation. *Cell* **144**(5), 646–674.

[6] Warburg O (1956). On the origin of cancer cells. *Science* **123**, 309–314 [80-.].

[7] Hennessy BT, Smith DL, Ram PT, Lu Y, and Mills GB (2005). Exploiting the PI3K/AKT pathway for cancer drug discovery. *Nat Rev Drug Discov* **4**(12), 988–1004.

[8] Chance B, Schoener B, and Oshino R (1979). Oxidation-reduction ratio studies of mitochondria in freeze-trapped samples. NADH and flavoprotein fluorescence signals. *J Biol Chem* **254**, 4764–4771.

[9] Ostrander JH, McMahon CM, Lem S, Millon SR, Brown JQ, Seewaldt VL, and Ramanujam N (2010). Optical redox ratio differentiates breast cancer cell lines based on estrogen receptor status. *Cancer Res* **70**(11), 4759–4766.

[10] Walsh AJ, Cook RS, Manning HC, Hicks DJ, Lafontant A, Arteaga CL, and Skala MC (2013). Optical metabolic imaging identifies glycolytic levels, subtypes, and early-treatment response in breast cancer. *Cancer Res* **73**(20), 6164–6174.

[11] Lakowicz J (1999). Principles of fluorescence spectroscopy. New York: Plenum Publishers; 1999.

[12] Lakowicz JR, Szmacinski H, Nowaczyk K, and Johnson ML (1992). Fluorescence lifetime imaging of free and protein-bound NADH. *Proc Natl Acad Sci U S A* **89**(4), 1271–1275.

[13] Nakashima N, Yoshihara K, Tanaka F, and Yagi K (1980). Picosecond fluorescence lifetime of the coenzyme of D-amino acid oxidase. *J Biol Chem* **255**(11), 5261–5263.

[14] So PTC, Dong CY, Masters BR, and Berland KM (2000). Two-photon excitation fluorescence microscopy. *Annu Rev Biomed Eng* , 399–429.

[15] Shannon C (1948). A mathematical theory of communication. *Bell Syst Tech J* **27**, 379–423.

[16] Magurran A (2004). Measuring biological diversity. Malden: Blackwell; 2004 .

[17] Marusyk A, Tabassum DP, Altrock PM, Almendro V, Michor F, and Polyak K (2014). Non-cell-autonomous driving of tumour growth supports sub-clonal heterogeneity. *Nature* **514**(7520), 54–58.

[18] Almendro V, Kim HJ, Cheng Y-K, Gönen M, Itzkovitz S, Argani P, van Oudenaarden A, Sukumar S, Michor F, and Polyak K (2014). Genetic and phenotypic diversity in breast tumor metastases. *Cancer Res* **74**(5), 1338–1348.

[19] Slack MD, Martinez ED, Wu LF, and Altschuler SJ (2008). Characterizing heterogeneous cellular responses to perturbations. *Proc Natl Acad Sci U S A* **105**(49), 19306–19311.

[20] Bendall S C, Simonds E F, Qiu P, Amir E D, Krutzik P O, Finck R, Bruggner R V, Melamed R, Trejo A, and Ornatsky O I, et al (2011). Single-cell mass cytometry of differential. **332**, 687–697.

[21] Amir ED, Davis KL, Tadmor MD, Simonds EF, Levine JH, Bendall SC, Shenfeld DK, Krishnaswamy S, Nolan GP, and Pe'er D (2013). viSNE enables visualization of high dimensional single-cell data and reveals phenotypic heterogeneity of leukemia. *Nat Biotechnol* **31**(6), 545–552.

[22] Skvortsova I, Skvortsov S, Raju U, Stasyk T, Riesterer O, Schottdorf E-M, Popper B-A, Schiestl B, Eichberger P, and Debbage P, et al (2010). Epithelial-to-mesenchymal transition and c-myc expression are the determinants of cetuximab-induced enhancement of squamous cell carcinoma radioresponse. *Radiother Oncol* **96**(1), 108–115.

[23] Tijink BM, Neri D, Leemans CR, Budde M, Dinkelborg LM, Stigter-van Walsum M, Zardi L, and van Dongen GA (2006). Radioimmunotherapy of head and neck cancer xenografts using 131I-labeled antibody L19-SIP for selective targeting of tumor vasculature. *J Nucl Med* **47**(7), 1127–1135.

[24] Joschko MA, Webster L K, Bishop J F, Groves J, Yuen K, Olver I N, Narayan K N, and Ball D L (1997). Radioenhancement by cisplatin with accelerated fractionated radiotherapy in a human tumour xenograft. *Cancer Chemother Pharmacol* **40**(6), 534–539.

[25] Skala MC, Riching KM, Gendron-Fitzpatrick A, Eickhoff J, Eliceiri KW, White JG, and Ramanujam N (2007). In vivo multiphoton microscopy of NADH and FAD redox states, fluorescence lifetimes, and cellular morphology in precancerous epithelia. *Proc Natl Acad Sci U S A* **104**(49), 19494–19499.

[26] Bird DK, Yan L, Vrotsos KM, Eliceiri KW, Vaughan EM, Keely PJ, White JG, and Ramanujam N (2005). Metabolic mapping of MCF10A human breast cells via multiphoton fluorescence lifetime imaging of the coenzyme NADH. *Cancer Res* **65**(19), 8766–8773.

[27] Shah A T, Demory Beckler M, Walsh A J, Jones W P, Pohlmann P R, and Skala M C (2014). Optical metabolic imaging of treatment response in human head and neck squamous cell carcinoma. *PLoS One* **9**(3), e90746.

[28] Walsh A J and Skala M C (2014). An automated image processing routine for segmentation of cell cytoplasms in high-resolution autofluorescence images. *SPIE Proc*, 89481M.

[29] Walsh A J and Skala M C (2015). Optical metabolic imaging quantifies heterogeneous cell populations. *Biomed Opt Express* **6**(2), 559.

[30] Diggins KE, Ferrell PB, and Irish JM (2015). Methods for discovery and characterization of cell subsets in high dimensional mass cytometry data. *Methods* **82**, 55–63.

[31] Kotecha N, Krutzik P O, and Irish J M (2010). Web-based analysis and publication of flow cytometry experiments. In: Robinson J P, editor. Current protocols in cytometry; 2010.

[32] Szollosi J, Balazs M, Feuerstein B, Benz C, and Waldman F (1995). ERBB-2 (HER2Ineu) gene copy number, p185HER2 overexpression, and intratumor heterogeneity in human breast Cancer. *Cancer Res* **55**, 5400–5407.

[33] Baselga B J, Pfister D, Cooper M R, Cohen R, Burtness B, Bos M, Andrea G D, Seidman A, Norton L, and Gunnett K, et al (2000). Phase I studies of anti – epidermal growth factor receptor chimeric antibody C225 alone and in combination with cisplatin. **18**(4), 904–914.

[34] Burtness B, Goldwasser MA, Flood W, Mattar B, and Forastiere AA (2005). Phase III randomized trial of cisplatin plus placebo compared with cisplatin plus cetuximab in metastatic/recurrent head and neck cancer: an Eastern Cooperative Oncology Group study. *J Clin Oncol* **23**(34), 8646–8654.

[35] Li X and Fan Z (2010). The epidermal growth factor receptor antibody cetuximab induces autophagy in cancer cells by downregulating HIF-1alpha and Bcl-2 and activating the beclin 1/hVps34 complex. *Cancer Res* **70**(14), 5942–5952.

[36] Berndtsson M, Hägg M, Panaretakis T, Havelka AM, Shoshan MC, and Linder S (2007). Acute apoptosis by cisplatin requires induction of reactive oxygen species but is not associated with damage to nuclear DNA. *Int J Cancer* **120**(1), 175–180.

[37] Asselin E, Mills G B, and Tsang B K (2001). XIAP regulates Akt activity and caspase-3-dependent cleavage during cisplatin-induced apoptosis in human ovarian epithelial cancer cells; 2001 1862–1868.

[38] Bernier J, Bentzen SM, and Vermorken JB (2009). Molecular therapy in head and neck oncology. *Nat Rev Clin Oncol* **6**(5), 266–277.

[39] Kimura H, Sakai K, Arao T, Shimoyama T, Tamura T, and Nishio K (2007). Antibody-dependent cellular cytotoxicity of cetuximab against tumor cells with wild-type or mutant epidermal growth factor receptor. *Cancer Sci* **98**(8), 1275–1280.

[40] Fodor IK (2002). A survey of dimension reduction techniques. US Dep. Energy; 2002.